

1       **Validation of European Land Data Assimilation System (ELDAS)**

2                               **products using *in situ* observations**

3  
4       **C.M.J. Jacobs<sup>1</sup>, E.J. Moors<sup>1</sup>, H.W. Ter Maat<sup>1</sup>, A.J. Teuling<sup>2</sup>, G. Balsamo<sup>3,4</sup>, K.**  
5       **Bergaoui<sup>3</sup>, J. Ettema<sup>4,5</sup>, M. Lange<sup>6</sup>, B.J.J.M. Van Den Hurk<sup>7</sup>, P. Viterbo<sup>4,8</sup>, and**

6                               **W. Wergen<sup>6</sup>**

7  
8                               *Alterra, Droevendaalsesteeg 3*

9                               *P.O. Box 47, 6700 AA Wageningen, The Netherlands*

10                               *cor.jacobs@wur.nl*

11  
12       1) Alterra, Wageningen, The Netherlands

13       2) Wageningen University, Hydrology and Quantitative Water Management Group, Wageningen  
14       The Netherlands

15       3) Météo-France-CNRM, Toulouse, France

16       4) European Centre for Medium-Range Weather Forecasts, Reading, UK

17       5) Utrecht University, Institute for Marine and Atmospheric Research, Utrecht, The  
18       Netherlands

19       6) Deutscher Wetterdienst, Offenbach, Germany

20       7) Royal Netherlands Meteorological Institute, De Bilt, The Netherlands

21       8) Instituto de Meteorologia, Lisboa, Portugal

22 **ABSTRACT**

23 Soil moisture products from land-surface data assimilation (DA) systems implemented at three  
24 European Weather Centers are validated. The DA systems are applied online, using the Soil-  
25 Vegetation-Atmosphere-Transfer (SVAT) models ISBA (Météo France), TERRA (German Weather  
26 Service) and TESSEL (European Centre for Medium-range Weather Forecasts), respectively. Output is  
27 compared to *in situ* observations from various databases. The present validation focuses on 1) soil  
28 moisture in the upper meter of the soil; 2) net precipitation, that is, precipitation minus  
29 evapotranspiration; 3) evaporative fraction. In the period considered here (May-October 2000) the DA  
30 systems generally add water. This considerably reduces bias in net precipitation, while the root mean  
31 square error of this quantity is slightly reduced as well. Evaporative fraction is improved in dry  
32 conditions in particular, but is hardly affected in moist conditions. The DA systems tend to cause  
33 underestimation of the amplitude of soil moisture variation. Properties of the land surface such as Leaf  
34 Area Index and water holding capacity of the soil are likely to control model results as well as the  
35 impact of the DA system. Depending on the application, improving the representation of such  
36 characteristics in the models may have greater priority than further improvement of the DA system.

37

## 38 **1 Introduction**

39 Soil moisture is a crucial state variable in Numerical Weather Prediction (NWP) models with  
40 realistic Soil-Vegetation-Atmosphere Transfer (SVAT) schemes. It controls to a large extent the  
41 partitioning of energy available at the surface between sensible and latent heat fluxes, and therefore  
42 the development of the atmospheric boundary layer (Ek and Holtslag, 2004; Santanello et al., 2005,  
43 Betts and Viterbo, 2005). However, typical time-scales of moisture changes in the upper meter of  
44 the soil are much longer than that of changes in tropospheric humidity. Incorrect initialization of  
45 soil moisture in NWP models may therefore result in systematic drift in the soil wetness state  
46 (Viterbo, 1996) and hence lead to poor model forecasts (Rhodin et al., 1999) (resilient errors).

47 At present, the complexity of the NWP systems precludes physically sound and yet feasible  
48 solutions to avoid drift of soil moisture in the SVAT schemes. Soil moisture assimilation is  
49 regarded as a pragmatic solution to repair biases in land – atmosphere interaction models related to  
50 soil wetness state (Van den Hurk and Ettema, 2007). In meteorological applications, the technique  
51 has been applied routinely since the mid-nineties (Mahfouf, 1991; Van den Hurk et al., 1997;  
52 Houser et al., 1998; Douville et al., 2000; Hess, 2001; Balsamo et al., 2004). Control of drift in soil  
53 moisture by land surface data-assimilation can considerably reduce forecast errors in screen-level  
54 temperature and humidity (Hess, 2001; Viterbo, 1996).

55 The research project “Development of a European Land Data Assimilation System to predict Floods  
56 and Droughts” (ELDAS) aimed to combine European expertise in the field of land-data assimilation  
57 and to develop and test a system to generate high-quality estimates of regional (European) scale soil  
58 moisture fields (Van den Hurk, 2002). It was related to the Global Land Data Assimilation System  
59 (GLDAS; Rodell et al., 2004) and the North American Land Data Assimilation System (NLDAS;  
60 Mitchell et al., 2004).

61 ELDAS systems were designed at three European NWP centers, and implemented in an online  
62 mode, that is, with full coupling to the NWP models. The latter feature is crucial, since it allows  
63 screen level observations to be used to drive the Data Assimilation (DA) system. It is necessary to

64 include such indirect measures of soil moisture status, because direct soil moisture observations are  
65 not readily available on a routine basis (Van den Hurk and Ettema, 2007).

66 The DA systems were applied within the SVAT schemes that are incorporated in the main  
67 operational NWP models of the three centers involved in the present study. The first SVAT model,  
68 ISBA (Interactions between the Soil, Biosphere and Atmosphere; Noilhan and Mahfouf, 1996) has  
69 been developed at the National Centre for Meteorological Research (CNRM), Météo-France. The  
70 second model, TERRA (Doms et al., 2005) has been developed at the German Weather Service  
71 (DWD). The third model, TESSEL (Tiled ECMWF Scheme for Surface Exchanges over Land; Van  
72 den Hurk et al., 2000) has been developed at the European Centre for Medium Range Weather  
73 Forecasts (ECMWF). Hereafter, the respective DA schemes will be named after the SVAT models  
74 applied at the NWP centers. For details on the DA and SVAT schemes the reader is referred to the  
75 cited literature.

76 The present paper describes a validation of the DA systems applied in ISBA, TERRA and TESSEL,  
77 respectively. Key-features of the SVAT and DA systems relevant to the present validation study  
78 will be given in Section 2. The systems are validated using *in situ* observations from 33 locations in  
79 Europe. The validation data originate from various databases that are briefly described in Section 3.  
80 The information content of these datasets varies widely among the locations, necessarily implying a  
81 different validation focus for the respective datasets. In order to focus the validation, three main  
82 topics were selected. Soil moisture, the quantity that is directly affected by the ELDAS system was  
83 selected as the first focus. Direct observations of soil moisture are only available from a limited  
84 number of sites. Therefore, as a second focus the behavior of net precipitation was chosen. Here,  
85 this quantity is defined as gross precipitation ( $P$ ) minus evapotranspiration ( $E$ ). For the validation  
86 period selected (May-October 2000), it is a major component of the soil hydrological balance, so  
87 that trends in  $P-E$  may be considered as a first-order approximation of trends in soil moisture. The  
88 third focus was chosen to be the energy partitioning at the surface, which plays a crucial role in  
89 meteorological models (see, e.g., Ek and Holtslag, 2004). Ultimately, land data assimilation systems

90 are designed to yield a correct energy partitioning in the meteorological models. The results of the  
91 validation for the three main topics are presented and discussed in Section 4. Finally, Section 5  
92 contains a general discussion and conclusions.

## 93 **2 Key features of the models and setup of the data assimilation experiment**

### 94 **2.1 General**

95 An overview of the SVAT schemes and the main layout of the DA experiment within ELDAS is  
96 given in Table 1. A full description of the physics of the SVAT schemes can be found in the cited  
97 literature. Here, only some key features of the DA experiment and characteristics that are crucial in  
98 the interpretation of the validation results are given.

99 The present validation study is restricted to the period May-October 2000, for which output from all  
100 models was available. ISBA and TERRA were run in their 3-dimensional mode. ISBA was run in  
101 the ARPEGE global model (Courtier et al., 1991), which has a Gaussian varying grid size ranging  
102 between 17 and 25 km over the ELDAS domain (Balsamo et al., 2005). TERRA is run in the Lokal-  
103 Modell (LM; Doms and Schättler, 2002) at a horizontal resolution of 7 km. The model output from  
104 ISBA-ARPEGE and TERRA-LM was post-processed to be projected on the ELDAS grid (“nearest  
105 neighbor”). The ELDAS grid extended from [35° N, 15° W] to [72° N, 38° E], with a horizontal  
106 resolution of 0.2x0.2 degrees. By contrast, TESSEL was run in a single-column (1-dimensional)  
107 mode (TESSEL-SCM) in which advection is prescribed as a lateral boundary condition to  
108 compensate for the lack of 3-dimensional feedback. The horizontal advection terms are derived  
109 from re-analyzed meteorological fields (ERA-40, Uppala et al., 2005). TESSEL-SCM was run  
110 specifically for gridpoints corresponding to the 33 validation sites.

111 ISBA and TERRA construct their land-surface properties from the Ecoclimap database (Masson et  
112 al., 2003), while TESSEL utilizes GLCC (Loveland et al., 2000). For the forcings of the land-  
113 surface part, ISBA and TERRA relied on their model-derived precipitation ( $P$ ), shortwave and  
114 longwave radiation ( $SW$  and  $LW$ , respectively). TESSEL used the special ELDAS forcing databases  
115 for the precipitation (Rubel et al., 2005) and radiation fields (Meetschen et al., 2004), respectively.

116 In the case of ISBA, a correction to soil moisture was applied to account for the difference between  
 117 model precipitation and ELDAS precipitation forcing (Balsamo et al., 2004, 2005). All DA systems  
 118 diagnose deviations in the soil moisture fields from forecast errors in screen-level observations.  
 119 ISBA and TESSEL used temperature ( $T$ ) as well as relative humidity ( $RH$ ), but TERRA used  $T$   
 120 only.

## 121 2.2 Description of evapotranspiration in the models

122 All models compute the turbulent fluxes using the well-known resistance analogue. For  
 123 evapotranspiration,

$$124 \quad E = c_{veg} \frac{\Delta\rho_v}{r_a + r_s} [\text{kg m}^{-2}\text{s}^{-1}] \quad (1)$$

125 where  $c_{veg}$  [-] is some measure of the vegetation cover,  $\Delta\rho_v$  [ $\text{kg m}^{-3}$ ] is the difference in water vapor  
 126 density between the effective source height of water vapor and a reference level in the air, and  $r_a$  [ $\text{s}$   
 127  $\text{m}^{-1}$ ] and  $r_s$  [ $\text{s m}^{-1}$ ] are the aerodynamic and surface resistance, respectively. In the present context,  $r_s$   
 128 has some special importance, because it incorporates the connection between soil moisture and the  
 129 conditions at the screen level. For vegetation,

$$130 \quad r_s = \frac{r_{s,min}}{LAI} \prod_{i=1}^n f^{-1}(x_i) \quad (2)$$

131 where  $r_{s,min}$  [ $\text{s m}^{-1}$ ] is the minimum stomatal resistance under optimal conditions,  $LAI$  [ $\text{m}^2 \text{m}^{-2}$ ] is the leaf  
 132 area index and  $f(x_i)$  are dimensionless empirical functions that account for the effect of environmental  
 133 conditions on stomatal aperture (Jarvis, 1976). Differences in  $r_s$  implied by differences in  $f(x_i)$  will cause  
 134 the main difference in the behavior of the modeled  $E$ . The function  $f(\theta)$  describing the impact of soil  
 135 moisture on  $r_s$  determines the sensitivity of screen level parameters to soil moisture conditions  
 136 (Mahfouf, 1991). The performance of the DA schemes will therefore be sensitive to  $f(\theta)$ .

## 137 2.3 Coupling between soil moisture, evapotranspiration and screen level observations

138 The link between the screen level observations and soil moisture is provided by evaporative  
 139 fraction,  $\mathcal{A}$ , defined as

140 
$$\Lambda \equiv \frac{\lambda E}{H + \lambda E} \quad (3)$$

141 where  $H$  [ $\text{W m}^{-2}$ ] is the sensible heat flux and  $\lambda$  [ $\text{J kg}^{-1}$ ] is the latent heat of vaporization. This link  
 142 can be further examined by re-writing the sensitivity equation for  $\lambda E$  to  $r_s$  given by Jacobs and De  
 143 Bruin (1992) as:

144 
$$\frac{\partial \Lambda}{\partial r_s} = \frac{-\Lambda}{(1 + s/\gamma)r_a + r_s} \quad (4)$$

145 which can readily be derived from the well-known Penman-Monteith equation. Here,  $s$  [ $\text{kg kg}^{-1}\text{K}^{-1}$ ]  
 146 is the slope of the saturation specific humidity versus temperature curve and  $\gamma[\text{K}^{-1}] \equiv c_p/\lambda$  is the  
 147 psychrometric constant, where  $c_p$  [ $\text{J kg}^{-1} \text{K}^{-1}$ ] is the specific heat capacity of the air. Equation (4)  
 148 represents the change in  $\Lambda$  per unit change in  $r_s$ . In the models considered here, the response of  $r_s$  to  
 149 soil moisture is modeled using in (2):

150 
$$f(\theta) = \begin{cases} 0 & \theta < \theta_w \\ \frac{\theta - \theta_w}{\theta_c - \theta_w} & \theta_w \leq \theta < \theta_c \\ 1 & \theta \geq \theta_c \end{cases} \quad (5)$$

151 where  $\theta_w$  [ $\text{m}^3 \text{m}^{-3}$ ] is the wilting point and  $\theta_c$  [ $\text{m}^3 \text{m}^{-3}$ ] a critical moisture content defining the  
 152 transition between supply and demand limited transpiration. ISBA and TESSEL assume  $\theta_c$  to be  
 153 equal to the field capacity  $\theta_{fc}$  [ $\text{kg m}^{-3}$ ], by which the second member of (5) becomes equal to the  
 154 Soil Water Index. In TERRA  $\theta_c$  is the so-called turgor loss point which is computed dynamically as  
 155 a function of the water holding capacity and the potential evaporation, following (Denmead and  
 156 Shaw, 1962). By virtue of (5),  $r_s$  and  $\Lambda$  are sensitive to  $\theta$  only in the range  $\theta_w \leq \theta < \theta_c$ . Because of  
 157 absence of synergy in (2), the modeled sensitivity of  $r_s$  to  $\theta$  in this interval can to first order be  
 158 written:

159 
$$\frac{\partial r_s}{\partial \theta} = \frac{-r_s}{\theta - \theta_w} \quad (6)$$

160 so that

161 
$$\frac{\partial \Lambda}{\partial \theta} = \frac{\Lambda}{\theta - \theta_w} (1 - \Omega) \quad (7)$$

162 with

163 
$$\Omega \equiv \left[ 1 + \frac{\gamma}{s + \gamma} \frac{r_s}{r_a} \right]^{-1} \quad (8)$$

164  $\Omega$  is the decoupling factor (Jarvis and McNaughton, 1986), describing to what extent the surface  
 165 and the conditions at a reference level are coupled. It attains values between 0 and 1 and is mainly  
 166 influenced by the surface characteristics implicit in  $r_s$  and  $r_a$ . It is further modulated by temperature,  
 167 through the dependence of  $s$  on temperature.

168 Equation (7) provides a justification of DA approaches where forecast errors in screen level  
 169 observations are used to diagnose soil moisture deviations and to improve the energy partitioning by  
 170 adjusting the soil moisture. The required sensitivity is present in the models by virtue of stress  
 171 function (5). Apart from the somewhat intuitive result that  $\Lambda$  should decrease with decreasing soil  
 172 moisture, (7) shows that the impact of soil moisture changes on  $\Lambda$  is expected to be largest for well-  
 173 coupled surfaces such as forests (high  $r_s$ , low  $r_a$ ). The sensitivity is strongly enhanced by dry soils  
 174 in two ways: 1) by decreasing the soil moisture content which reduces  $\theta - \theta_w$ ; 2) by increasing  $r_s$   
 175 and therefore  $(1 - \Omega)$ . Thus, (7) implies that a given soil moisture increment will have a larger impact  
 176 on  $\Lambda$  in dry conditions than in wet conditions. Although the sensitivity represented by (7) will be  
 177 modulated by feedback with the ABL (Jacobs and De Bruin, 1992; Ek and Holtslag, 2004) this  
 178 equation can be used to interpret the main differences in the impact of the various DA systems on  
 179  $\Lambda$ .

## 180 **2.4 Water holding capacity**

181 In all cases, soil moisture is a relatively slowly varying variable. Of paramount importance is the  
 182 water-holding capacity, defined here as the difference between field capacity and wilting point for a  
 183 soil layer with depth 1 m. The water holding capacity depends on soil texture and differs  
 184 considerably among the models, as shown in Table 2. The amount of water available for



185 evapotranspiration is both a function of the water holding capacity as defined in Table 2 and of  
186 rooting depth.

187 The largest range in water holding capacity per unit soil depth is modeled in TERRA. Although  
188 ISBA computes wilting point and field capacity from the textural composition of the soils, the  
189 actual range of water holding capacity (~80 mm) is small. TESSEL uses one uniform soil type.

190 The minimum sensitivity of  $\lambda$  to soil moisture content is directly controlled by the water holding  
191 capacity, as can be seen from (7): the minimum sensitivity is obtained as  $\theta \rightarrow \theta_c$ . Note that then  
192  $f^{-1}(x_n) \rightarrow 1$ . For otherwise similar conditions the sensitivity is inversely proportional to the water  
193 holding capacity. Thus, under well-watered conditions and for similar rooting depth, the sensitivity  
194 of  $\lambda$  in ISBA may be expected to be roughly twice that of TESSEL, and 2-3 times that of TERRA.

### 195 **3 In situ observations and focus of the present validation study**

#### 196 **3.1 General**

197 Figure 1 shows the locations of the 33 validation sites, that is, sites where observational data used in  
198 the present validation study were collected. The observations were performed in the context of  
199 different field campaigns, set up with different purposes. Therefore, the information content of the  
200 data sets varies widely among the locations. Also, a large range of climatic conditions is represented  
201 in the data.

202 At 24 out of the 33 validation sites, direct soil moisture observations were performed. These sites  
203 are henceforth called “soil moisture sites”. Some of the soil moisture observations show great detail  
204 in space and time. At all soil moisture sites precipitation is measured. Occasionally, other  
205 observations such as soil temperature are available, but at most of the soil moisture sites turbulent  
206 fluxes of latent and sensible heat were not observed.

207 At 14 out of the 33 sites micrometeorological observations of the turbulent fluxes were performed.  
208 These sites will be referred to as “flux sites”. The flux measurements were generally accompanied  
209 by observations of meteorological variables such as temperature, humidity, and radiation. At the

210 majority of the sites, precipitation was observed as well. However, soil moisture was measured at a  
211 limited number of the flux sites only.

### 212 **3.2 Validation data sources**

213 In this study data from the following experiments were used:

#### 214 *a) The Danish Pesticide Leaching Assessment Programme (PLAP)*

215 This programme was designed to monitor the leaching behavior of pesticides or their degradation  
216 products to groundwater. At six PLAP monitoring sites detailed observations of soil moisture and  
217 temperature profiles were performed. The observations in the soil were accompanied by  
218 observations of precipitation. For a detailed description of the sites and the measurements the  
219 reader is referred to Lindhardt et al. (2001).

220

#### 221 *b) BALTEX-Estonia*

222 The Baltic Sea Experiment (BALTEX) is an international research initiative aimed at  
223 understanding the hydrological balance and energy exchange of the Baltic sea drainage basin  
224 (Raschke et al., 2001). For the ELDAS validation period, soil moisture content and precipitation  
225 data were made available for the Estonian region.

226

#### 227 *c) CarboEuroflux*

228 The major goal of the CarboEuroflux program is to improve the understanding of the magnitude  
229 and temporal and spatial variability of the carbon source and sink strengths of terrestrial  
230 ecosystems (Valentini et al., 2000). The main data available from these sites are observations of  
231 the turbulent fluxes, obtained following prescribed experiment and data processing protocols  
232 (Aubinet et al., 2000). For the ELDAS year 2000, observations of  $H$  and  $\lambda E$  were available at 13  
233 forested sites, distributed over the European continent. Precipitation was observed at all but one  
234 of the CarboEuroflux sites used here. At some sites, soil moisture content was observed at depths

235 below 20 cm and seasonal trends derived from these observations were included in the present  
236 analysis.

237

#### 238 d) *Scintillometer observations in Spain*

239 For one site in Spain, flux observations were available from the large scale Energy and Water  
240 Balance Monitoring System project (EWBMS; Moene and De Bruin 2001). These measurements  
241 were performed with a Large Aperture Scintillometer (LAS), in an irrigated area near Badajoz in  
242 Spain. LAS can be used to measure sensible heat flux  $H$  over distances of 5-10 km and can even  
243 be applied to determine average fluxes over the various surface types within the scintillometer  
244 path (Meijninger et al., 2002). However, because the LAS only measures  $H$  directly,  $\lambda E$  has to be  
245 derived from the surface energy balance:

$$246 \quad \lambda E = Q_* - G - H \quad (9)$$

247 where  $Q_*$  [ $\text{W m}^{-2}$ ] is the net radiation and  $G$  [ $\text{W m}^{-2}$ ] is the soil heat flux. Observations of  
248 precipitation and the amount of irrigation in the scintillometer area were also available.

### 249 **3.3 Validation focus and processing of the data**

250 In accordance with the differing information content of the validation datasets, three main  
251 validation topics were chosen.

#### 252 a) *Soil moisture*

253 Soil moisture is directly affected by the ELDAS systems and was therefore selected as the first  
254 focus. In order to avoid disparities due to the different discretization of the models, the moisture  
255 content in the upper 1m of the soil ( $\theta_{1m}$  [ $\text{m}^3 \text{m}^{-3}$ ]) was considered. At some validation sites  $\theta_{1m}$  was  
256 observed directly. Analysis of detailed data from these sites showed that normalized trends of  $\theta_{1m}$   
257 can be approximated by normalized trends from observations below a depth of 20 cm. Therefore,  
258 such approximations of the trend in  $\theta_{1m}$  were used for locations where direct observations of  $\theta_{1m}$   
259 were not available.

260 In order to ensure a fair comparison between observations and modeled soil moisture, normalized  
 261 quantities are preferred and to this end, soil water index  $(\theta - \theta_w)/(\theta_{fc} - \theta_w)$  has often been used in the  
 262 past (e.g., Dirmeyer et al., 2000). However, for the validation sites  $\theta_{fc}$  and  $\theta_w$  were often lacking.  
 263 Another option is to compute an index from the maximum and minimum soil moisture value in a  
 264 given period. However, this normalization is sensitive to rare extremes and exaggerates normalized  
 265 trends in soil moisture. Moreover, dynamical differences are obscured, because any dataset will  
 266 give normalized ranges between 0 and 1. For these reasons, it was decided to normalize the  
 267 computed or observed values of the  $\theta_{lm}$  using the 95-percentile value  $\theta_{lm}^{95}$  of the validation period:

$$268 \quad \hat{\theta} = \frac{\theta_{lm}}{\theta_{lm}^{95}} \quad (10)$$

269 This normalization is less sensitive to a few rare extremes, while still allowing an examination of  
 270 differences in trends.

271

#### 272 b) Net Precipitation, $P-E$

273 For none of the validation sites observations of natural drainage and runoff were available, which  
 274 precluded analyses of the full soil hydrological balance. However, for the period under  
 275 consideration gross precipitation and evapotranspiration,  $P$  and  $E$ , respectively, may be regarded as  
 276 the major components of the soil hydrological balance at most validation sites. Therefore, the net  
 277 input  $P-E$  was chosen as the second main focus of the present study.  $P-E$  can be used to evaluate the  
 278 performance of the DA system as follows.

279 Within the model framework the soil hydrological balance of a layer with given depth for a given  
 280 period of time of one day, say, is given by

$$281 \quad \Delta W = P - E + \delta W - (R + D) \quad (11)$$

282 where  $W$  is the bulk soil moisture content,  $\delta W$  denotes the increments from the data assimilation  
 283 system,  $R$  is runoff and  $D$  is drainage. For the observations  $\delta W$  is zero. Assuming  $(R+D) \ll (P-E)$ ,  
 284 the effect of the DA system can therefore be assessed by comparing  $P-E$  from the observations with

285  $P-E+\delta W$  and  $P-E$ , respectively, from the models. Because this analysis requires  $E$ , it could only be  
286 performed for flux sites. Cumulative values of  $P$ ,  $E$ , and  $\delta W$  over periods of one month are  
287 considered. By resetting sums to zero each month, propagation of errors in early months to later  
288 months is avoided. Furthermore, specific seasonal features of the performance can be revealed.  
289 Observed  $P$  was taken from the ELDAS precipitation database (Rubel et al., 2005). This database  
290 consists of 3-hourly precipitation sums for each gridpoint in the ELDAS domain, constructed from  
291 over 20000 rain gauge observations and radar observations in Europe. This data source is preferred  
292 over the local observations, because it guarantees high-quality observations of  $P$  to be available for  
293 all sites, at all times in the validation period. Furthermore, it matches the spatial scale of the model  
294 resolution and the quality of the ELDAS precipitation database is probably best in the period that is  
295 considered here (Rubel et al., 2005).

296

### 297 c) *Evaporative fraction, $\Lambda$*

298 The third major focus of the present validation study was chosen to be  $\Lambda$ , defined by (3). It is an  
299 important diagnostic in land-surface schemes (Ek and Holtslag, 2004; Betts and Viterbo, 2005), and  
300 may also serve as a soil-moisture indicator (Bastiaanssen, 1995).  $\Lambda$  quantifies the partitioning of  
301 available energy between heating and moistening the Atmospheric Boundary Layer (ABL). It  
302 controls to a large extent the ABL dynamics, including the formation of clouds within the ABL (Ek  
303 and Holtslag, 2004; Betts and Viterbo, 2005). Because it is a normalized flux,  $\Lambda$  allows a fair  
304 comparison between the model and the observations, independent of differences between prescribed  
305 and real surface characteristics. Also note that  $\Lambda$  is less sensitive to possible energy balance closure  
306 problems from the EC measurements.

307 Obviously, only data from flux sites could be used in this analysis. Data treatment from these sites  
308 needed special care in order to ensure meaningful analyses of  $\Lambda$ . Apart from the basic quality  
309 requirements within the CarboEuroflux community (Aubinet et al., 2000), the data were post-  
310 processed as follows.

311 Daily values of  $\lambda$  were computed for every flux site ( $n=14$ ) using only mean hourly values of  $H$  and  
312  $\lambda E$  between 10 and 15 UTC. For the sites considered here, the selected daytime period contains  
313 local noon in all cases. Observations were excluded if precipitation had occurred during the  
314 averaging period, and if the observed wind speed was less than 1 m/s. For both the model and the  
315 observations it was also required that  $H > -20 \text{ W/m}^2$  and  $\lambda E > 10 \text{ W/m}^2$  (with upward fluxes taken  
316 positive). These requirements exclude extremely stable conditions under which  $\lambda$  is a poor indicator  
317 of soil wetness and boundary layer dynamics. Finally,  $\lambda$  for a specific day was included only if it  
318 could be computed from at least 4 out of 5 hourly flux values after the aforementioned data  
319 screening procedure.

320 For each flux site, average monthly differences between modeled and observed  $\lambda$  were computed if  
321 in a particular month at least 50% of the noontime differences was available at that site. Next, for  
322 each month the mean differences were averaged over all sites with sufficient data in that month.  
323 October was excluded in all cases, because in that month  $\lambda$  usually played no meaningful role as a  
324 soil moisture indicator anymore. Wet conditions due to precipitation often led to a stably stratified  
325 atmosphere in this month so that only a small number high-quality  $\lambda$  values could be obtained.

326

## 327 **4 Results**

### 328 **4.1 Soil moisture**

329 Figure 2 shows the normalized soil moisture content  $\hat{\theta}$  as defined by (10) typical of Vielsalm,  
330 Belgium, and El Saler, Spain. The general features of these cases are representative of moist and  
331 dry locations, respectively. It can be seen that the models are quite capable of simulating the  
332 situation in the moist case of Vielsalm. The amplitude of the variation in  $\hat{\theta}$  is limited for both the  
333 observations and the models and amounts to, roughly, 0.40. Also, the timing of the variations is  
334 reasonably well simulated. In contrast,  $\hat{\theta}$  is generally overestimated for the dry case of El Saler,

335 except when a rainfall event causes the observed soil moisture to increase. Rapid increases in  $\hat{\theta}$  due  
336 to rainfall events are observed, but not simulated by the models. An exception is the rainfall event  
337 on DOY (Day Of Year) 295 that has a clear impact on the output from ISBA and TESSEL. While  
338 the soil is observed to quickly dry out after a rainfall event, with values of  $\hat{\theta}$  dropping to between  
339 0.1 and 0.3, the models maintain the soil wetness at a high level with  $\hat{\theta}$  between 0.6 and 0.8.  
340 Analysis of the soil hydrological balance after a rainfall event suggests that the high values are due  
341 to the addition of soil water by the DA system. Table 3 highlights the balance terms in the period  
342 between DOY 162 and DOY 191, just after the rainfall event on DOY 161. On DOY 162,  $\hat{\theta}$  is  
343 about equal for the observations and the models. Hereafter, there hardly any precipitation is  
344 observed and the soil dries out. For all three schemes, the computed evapotranspiration is too high.  
345 However, in the case of ISBA, the output of soil water by evapotranspiration is fully compensated  
346 by input of water from the DA scheme and the soil water content increases. For TERRA, the  
347 compensation of evapotranspiration by the DA scheme amounts to 75%. This suggests that in these  
348 models, the amplitude of  $\hat{\theta}$  is almost entirely limited by the DA scheme in the case of El Saler. For  
349 TESSEL, the compensation of evapotranspiration by the DA scheme is some 40%. However, the  
350 evapotranspiration term is overestimated much less than in the case of ISBA and TERRA. As a  
351 result, the modeled net loss of water from the soil (42 mm) corresponds quite well with the  
352 observed one (39 mm).

353 The underestimated amplitude of  $\hat{\theta}$  at El Saler might be an important characteristic of the DA  
354 schemes investigated here. Therefore, the modeled and observed seasonal amplitude of  $\hat{\theta}$  was  
355 compared for all validation sites where direct or approximated trend of  $\theta_{Im}$  could be calculated (22  
356 sites). The amplitude is computed simply as the difference between the normalized minimum and  
357 maximum of the daily  $\hat{\theta}$  values in the validation period May-October 2000. Thus, it contains  
358 information on the amplitude of the seasonal cycle as well as on trends at shorter timescales such as  
359 induced by precipitation (see the El Saler example discussed above).

360 Results are shown in Figure 3. Amplitudes  $> 0.5$  are quite common in the observed values. TERRA  
361 is the only model capable to mimic such amplitudes, with values up to about 0.65. However,  
362 inspection of a number of cases revealed that the timing of the minima and maxima was quite  
363 wrong (not shown here). Moreover, modeled amplitudes did not always match observed amplitudes  
364 for specific sites (Fig. 3). Amplitudes of ISBA and TESSEL remain below 0.3 for all sites.

365 It is concluded that the models tend to underestimate the amplitude of soil water content. The  
366 analysis for El Saler shows that this may be partly due to the influence of the DA scheme, which  
367 limits drying of the soil. In addition, soil physical characteristics may limit modeled amplitudes of  
368 soil moisture. The larger water holding capacity of TERRA (see Table 2) could explain the larger  
369 amplitude of the soil moisture simulated by this model.

370 For completeness, the non-normalized amplitude, expressed in mm of water per meter of soil, was  
371 also investigated. The results, shown in Figure 4 improved the comparison with the observations for  
372 ISBA and TESSEL, although there was still an underestimation on average, while there was a slight  
373 tendency to overestimate the amplitude in the case of TERRA. It is important to realize that  
374 discrepancies in the modeled soil hydrological balance do not necessarily imply a mismatch of  
375 evapotranspiration, due to compensating factors, such as a too small water holding capacity with too  
376 large rooting depth, or influence of drainage and runoff, which are not analyzed at present.

## 377 **4.2 Net Precipitation**

378 For the flux sites with direct observations of evapotranspiration (14 sites) observed  $P-E$  was  
379 computed for all months of the validation period (May-October). Figure 5 shows an example of  $P-E$   
380 and  $P-E+\delta W$  for validation site Flakaliden in Sweden. The results for this particular site illustrate a  
381 couple of quite typical features of the ELDAS systems. Comparing the balance terms with and  
382 without  $\delta W$  shows that in some months the DA scheme improves the modeled soil hydrological  
383 balance, in others it does not. TESSEL performs rather well over the entire period and the  
384 increments improve the performance a little further. However, recall that  $P$  from ELDAS is one of  
385 the direct forcings of TESSEL. In contrast, the DA scheme of TERRA seems to deteriorate the



386 output of this model. While the initial estimate of  $P-E$  agrees reasonably well with the observations  
387 the results for  $P-E+\delta W$  are much worse. This adverse effect of the DA scheme in TERRA was  
388 found in a number of other cases as well, and seems to be typical for the first one or two months,  
389 not for the third and subsequent months. This is probably an effect of spin-up as the assimilation  
390 was initially started from interpolated fields from a global model that has a free-running soil  
391 (Wergen et al., 2005). The output from ISBA is significantly improved by the DA scheme.  
392 However, the main improvement is due to the soil moisture correction based on the precipitation  
393 bias. The relatively poor estimate of  $P-E$  from ISBA was mainly due to the fact that  $P$  was quite far  
394 off in this case (*not* typical for all sites). These deviations triggered large  $P$ -related corrections in  
395 the ISBA scheme, that considerably improved the modeled soil hydrological balance. In some  
396 cases, this correction completely cancelled the increments due to the 2d-Var component of the DA  
397 scheme in ISBA.

398 For the flux sites, monthly cumulative observed  $P-E$  was compared to modeled  $P-E$  and  $P-E+\delta W$ ,  
399 respectively, if the data coverage of observed  $E$  in a particular month was at least 67% ( $n=13$  for  
400 May-June;  $n=12$  for July-October). Mean monthly bias of  $P-E$  and  $P-E+\delta W$ , respectively, was  
401 computed as well as the root-mean-square-error (*rmse*) of the monthly sums from the differences at  
402 the validation sites. The monthly results are depicted in Figure 6. The averages over all months in  
403 the validation period are given in Table 4. A negative bias means that the model is too dry.

404 It can be seen that including the increments considerably reduced the bias in all models, in most  
405 months, suggesting a beneficial effect of the DA system on the soil hydrological balance. Only in  
406 October the DA system has hardly any effect on the bias in the monthly sums. In the case of  
407 TESSEL a gradual systematic decrease of the bias during the growing season can be seen. There is  
408 also a reduction of the *rmse*, of about 16% for ISBA, 15% for TESSEL but only about 5% for  
409 TERRA. This much lower improvement in the case of TERRA is related to the spin-up problems  
410 mentioned above and to the use of  $P$  from the model rather than from observations. The  
411 improvement in the case of ISBA is due mainly to the  $P$ -based correction. The effect on the *rmse* is

412 much less systematic than the effect on the bias. Some months show a clear improvement with  
413 respect to *rmse*, others do not. Again, the largest improvement in the case of TESSEL is obtained in  
414 the first part of the validation period and gradually decreases towards October.

### 415 **4.3 Evaporative Fraction**

416 The *rmse* of  $\Lambda$  on a monthly timescale was computed from the monthly averaged differences per  
417 site. The result is shown in Figure 7 for the individual months and in Table 5 for the seasonal mean.  
418 In addition, because of the role of  $\Lambda$  as a diagnostic of relatively fast dynamic boundary layer  
419 processes in NWP models, for each site the *rmse* in a particular month was also computed from  
420 daily errors if at least 15 error estimates were available. The *rmse* on this daily timescale, averaged  
421 over all sites is also shown in Figure 7. Moreover, Table 5 shows the seasonal mean of the *rmse* on  
422 a daily timescale.

423 The average bias of the models varies between 0.06 and 0.09. These numbers correspond to 12-17%  
424 of the average observed  $\Lambda$  (0.50, range 0.31-0.71). The *rmse* varies between 0.20 and 0.23 on the  
425 monthly timescale, and between 0.23 and 0.27 on the daily timescale, which corresponds to 40-46%  
426 and 46-54% of the average  $\Lambda$ . During the validation period, a seasonal cycle can be observed in the  
427 bias, but not in the *rmse*. The trend in the bias seems to be somewhat similar for ISBA and  
428 TESSEL, with minimum deviations in July-August, but TERRA shows a reversed trend with a  
429 maximum deviation in June-July.

430 The influence of the DA system on the quality of  $\Lambda$  cannot be evaluated from the information given  
431 above. Only in the case of TESSEL a control run without data assimilation was performed. A  
432 limited screening of the effect was performed for this model by comparing the output from the  
433 control run and the DA run in a dry and a moist situation (see Van den Hurk and Ettema, 2007, for a  
434 more extensive discussion of the increments). The differences between dry and moist conditions  
435 should lead to quite different impacts of the DA systems (see Section 2.3). Figure 8 shows the 11-  
436 day moving average of the noontime  $\Lambda$  for El Saler (Spain, dry case) and Soroe (Denmark, wet

437 case), respectively, for the observations, TESSEL with DA system, and the TESSEL control run. It  
438 can be seen that in the case of El Saler  $\lambda$  is too small in the control run, apart from the start of the  
439 period. In the DA run  $\lambda$  becomes too large. The overcorrection may be due in part to the high  
440 sensitivity of  $\lambda$  to soil moisture under dry conditions, that is implicit in all the models because of  
441 the root functions chosen. By contrast, in the case of Soroe  $\lambda$  is too high during most of the period.  
442 There is hardly any effect of the DA system on the performance of  $\lambda$  in this case, especially when  
443 considering the end of the period. Even smaller impacts on  $\lambda$  were found for other moist sites. The  
444 results are consistent with the conclusion from the sensitivity analysis that in the model context the  
445 sensitivity of  $\lambda$  to soil moisture increases under dry conditions.

446 The surface characteristics in the model, such as LAI, albedo, roughness and water holding  
447 capacity, differ from the real surface characteristics. Given the sensitivity of  $\lambda$  to such properties it  
448 may be argued that improvement of the modeled surface characteristics should be preferred over  
449 further improvement of the DA systems, especially under wet conditions where effects of the DA  
450 system are expected to be small (see Section 2.3). The possible impact on  $\lambda$  of improving *LAI* is  
451 illustrated for a number of stations in the Estonia, where TERRA displayed a clear seasonality in  $\lambda$ .  
452 For ISBA, the seasonal change of *LAI* is much smaller in this region, while TESSEL has a constant  
453 *LAI*.

454 Figure 9 shows the model results for the Jogeve site which is typical for the Estonian region. The  
455 Figure shows the modeled 11-day moving averages of  $\lambda$ , constructed from at least 6 daily values  
456 within the averaging interval. Because no flux sites are available in this area,  $\lambda$  was also computed  
457 using the well-known Priestley and Taylor (1972) approach, that gives reasonable estimates of  $\lambda E$   
458 for well-watered, dense grasslands and crops under optimal conditions. In spite of the temperature  
459 and radiation dependence,  $\lambda$  from the Priestley and Taylor approach ( $\lambda_{PT}$ ) shows hardly any  
460 seasonal dependence. However, because the approach is valid for dense vegetation, it implicitly  
461 excludes the influence of a varying *LAI*. In the next step, a dependence on *LAI* was therefore

462 included by scaling the Priestley and Taylor  $\lambda E$  with the  $LAI$  variation in the models, that is,  $\lambda E$  was  
463 reduced by a fraction  $LAI/LAI_m$ , where  $LAI_m$  is the maximum  $LAI$  of the season. This is consistent  
464 with increasing  $r_s$  in (2), like in the models. In this way,  $A_{PT}$  was scaled with  $LAI$  from ISBA and  
465  $LAI$  from TERRA, by using their monthly  $LAI$  values, linearly interpolated to daily  $LAI$  values. The  
466 results are also displayed in Figure 9.

467 Accounting for the seasonal variation in  $LAI$  explains much of the differences between the models,  
468 especially at the start of the period investigated here. Indeed, the impact of  $LAI$  on  $A_{PT}$  was much  
469 larger than the impact of the DA system on  $A$  in the case of TESSEL. The 11-day moving average  
470 of  $A$  from the TESSEL control run for Jogeva was almost identical to the DA run and is therefore  
471 not included in Figure 9.

## 472 **5 Discussion and conclusions**

473 In the present study the performance of a soil moisture DA scheme implemented in three  
474 operational SVAT schemes, ISBA (Météo-France), TERRA (Deutscher Wetter Dienst) and  
475 TESSEL (European Centre for Medium-Range Weather Forecasts) has been assessed in the context  
476 of ELDAS. The schemes were validated for the period May-October 2000, using *in situ*  
477 observations from 33 sites in Europe.

478 Assuming that  $P-E$  is the most important part of the soil hydrological balance over the period  
479 considered here allowed assessment of the performance of the DA scheme with respect to the soil  
480 hydrological balance by comparing  $P-E$  or  $P-E+\delta W$ , respectively, to the observed  $P-E$ . The DA  
481 systems of ISBA, TERRA and TESSEL generally add water to the soil, thereby reducing the bias in  
482  $P-E$  versus  $P-E+\delta W$  by at least a factor of four (Table 4). In addition, the *rmse* of the monthly sums  
483 is reduced by 15-16% for ISBA and TESSEL, but only by 5% in the case of TERRA. For the latter  
484 model, the performance in the first one or two months of the simulations becomes worse, which  
485 may be attributed to spin-up, and adversely affects the overall improvement. The improvement of  
486 the ISBA soil hydrological balance is mainly due to the soil moisture correction based on the

487 precipitation bias. On a monthly timescale, the impact of the DA increments based on screen level  
488 observations was much less and often almost neutralized by the precipitation corrections. The  
489 improvement of ISBA due to the precipitation corrections demonstrates the importance of high-  
490 quality precipitation fields. It also proves that assimilation of observed precipitation could be used  
491 to improve soil moisture fields in a physically consistent way.

492 The quality of the soil moisture simulations was assessed by considering soil moisture values  
493 normalized to the 95 percentile daily value of the validation period. The models underestimate the  
494 amplitude of the normalized soil moisture variations. As is demonstrated in the analysis of the soil  
495 water balance in El Saler (Fig 2, Table 3), this is partly due to the increments that keep the soils  
496 relatively wet. This result is consistent with the results of Bell et al. (2005), who found similar  
497 reductions of the amplitude in the context of a study on the effects of the DA system on river  
498 discharge.

499 Maximum normalized soil moisture variations are dictated by the water holding capacity of the soils  
500 incorporated in the models (Table 2). Because TERRA has the largest dynamical range in  
501 normalized soil moisture values between field capacity and wilting point, this model was capable of  
502 covering a major portion of observed soil moisture amplitudes. However, analysis of changes in  
503 non-normalized daily soil moisture values reveals that in many cases the total water exchange with  
504 the atmosphere may be much closer to the observed one than the amplitude of the normalized soil  
505 moisture values suggest. In a meteorological context, the exchange of water with the atmosphere is  
506 more important than the actual soil moisture status. Thus, in meteorological models the limited  
507 modeled soil moisture amplitude may still be considered acceptable.

508 Evaporative fraction  $\lambda$  is an important quantity in meteorological models because it diagnoses the  
509 energy partitioning at the Earth's surface, which again affects the development of the Planetary  
510 Boundary Layer (Ek and Holtslag, 2004). For the purpose of validation, it is also an attractive  
511 parameter, since it is a normalized flux that partly removes the difference between the model

512 surface characteristics and the real surface properties. Such differences would make a direct  
513 comparison of the turbulent fluxes, without normalization, unfair.

514 An average bias in  $\lambda$  of 0.06 – 0.085 was found, which is typically about 15% of the average  $\lambda$ . All  
515 three schemes displayed a seasonality of the bias. The cycle is different for TERRA than for ISBA and  
516 TESSEL, with the first model showing a maximum bias in June and July, and the latter models showing  
517 a minimum bias of about zero in July-August (Fig. 7). However, TERRA encountered spin-up  
518 problems in the first few months. The *rmse* was found to range between 0.2 and 0.23 on a monthly  
519 timescale (typically ~45% of  $\lambda$ ), and from 0.24-0.27 using daily noon values of  $\lambda$  (~50%). The *rmse*  
520 showed no consistent trend during the validation period.

521 Implementing a DA system can be viewed as a practical approach to improve model forecasts. In the  
522 present study the effect of the DA system on  $\lambda$  was assessed in the case of TESSEL, for moist and dry  
523 conditions, respectively. Hardly any improvement was found for the moist case, but  $\lambda$  for the dry case  
524 showed a significant improvement. This is consistent with the sensitivity analysis of Section 2.3: the  
525 present parameterizations of the vegetation response to soil moisture imply only small effects on  $\lambda$  of  
526 additional water under humid conditions. Rather than further improving the soil moisture assimilation  
527 system using observations that are only indirectly linked to  $\lambda$ , improving the physics and basic  
528 parameter fields should be attempted.

529 Even zonally averaged evapotranspiration is sensitive to seasonal trends in  $LAI$  (Van Den Hurk et al.,  
530 2003). Indeed, our analysis for the Estonian region (Fig. 9) revealed that the impact of  $LAI$  on  $\lambda$   
531 exceeded the impact of the DA scheme on  $\lambda$ . Therefore, under moist conditions, realistic prescription  
532 of  $LAI$  seems to be important. To improve evapotranspiration rates under dry conditions, alternative  
533 functions to describe water extraction by roots could be attempted. For example, including the ability  
534 of roots to actively deal with water shortage by increasing the capacity for water uptake (Teuling et al.,  
535 2006) would at least partially prevent  $\lambda$  from dropping to low values too soon. In order to maintain  
536 realistic soil moisture behavior an improved description of the soil properties should be included. This

537 option would not only be beneficial in a meteorological context, but also from the perspective of  
538 hydrological applications.

539 Only a few generalizations have been made here because of the following reasons. TERRA only  
540 used temperature as a diagnostic for deviations in soil moisture, while ISBA and TESSEL used  
541 temperature as well as relative humidity. Furthermore, the definition of soil and vegetation within  
542 the models was based on different databases and the forcings were different as well (see Table 1).  
543 Also, a single-column version of TESSEL was used that prescribes large-scale advection using  
544 results from the 3D model without the assimilation scheme. Thus, possible effects of the DA  
545 scheme on 3D interactions are implicitly ignored. The observation data base used to validate the DA  
546 schemes originated from different sources, implying large differences in their information content.  
547 At 24 out of 33 sites, direct soil moisture observations were available, often with very different  
548 characteristics in temporal and spatial resolution. At 14 out of the 33 sites flux observations were  
549 performed, but often no soil moisture observations were available. Also, most of the flux  
550 observations were performed over forest, and the sites tend to be located near the coast.

551 Because soil moisture is a crucial quantity in many models and parameterizations, direct validation  
552 of this quantity is preferred. Based on the experience in the present study, we would therefore  
553 strongly support the establishment of a network of standardized and quality-controlled soil moisture  
554 observations, preferably integrated in the existing flux-observation networks such as FLUXNET  
555 (Baldocchi et al., 2001).

556 In spite of the considerations given above, it is concluded that the soil moisture data assimilation  
557 systems can be regarded as a practical solution to improve model performance in some respects.  
558 From the meteorological point of view their effect is quite limited under humid conditions in  
559 particular. However, the impact of physical processes related to fundamental surface properties in  
560 the models, such as water holding capacity and *LAI*, suggests that improving such characteristics  
561 and the description of processes describing the water balance may be equally beneficial and may  
562 have greater priority than further improvement of the land surface data assimilation system.

563 **Acknowledgements**

564 This ELDAS research has been supported by the European Commission, contract EVG1-CT-2001-  
565 00050, and by Alterra B.V., Wageningen. We would like to thank the PI's and field workers of the  
566 CarboEuroflux and BALTEX communities for making available their data. Arnold Moene and  
567 Henk de Bruin of the Meteorology and Air Quality department of Wageningen University are  
568 thanked for allowing us to use the scintillometer data. We are indebted to Finn Lars Plauborg for  
569 making available the Danish PLAP data.

570

571 **References**

- 572 Aubinet, M., Grelle, A., Ibrom, A., Rannik, U., Moncrieff, J., Foken, T., Kowalski, A.S., Martin, P.H.,  
573 Berbigier, P., Bernhofer, C., Clement, R., Elbers, J., Granier, A., Grunwald, T., Morgenstern, K.,  
574 Pilegaard, K., Rebmann, C., Snijders, W., Valentini, R., Vesala, T., 2000. Estimates of the annual net  
575 carbon and water exchange of forests: The EUROFLUX methodology. *Advances in Ecological*  
576 *Research* **30**, 113-175.
- 577 Baldocchi, D., Falge, E., Gu, L., Olson, R., Hollinger, D., Running, S., Anthoni, P., Bernhofer, C., Davis, K.,  
578 Evans, R., Fuentes, J., Goldstein, A., Katul, G., Law, B., Lee, X., Malhi, Y., Meyers, T., Munger, W.,  
579 Oechel, W., Paw, K.T., Pilegaard, K., Schmid, H.P., Valentini, R., Verma, S., Vesala, T., Wilson, K.,  
580 Wofsy, S., 2001. FLUXNET: A New Tool to Study the Temporal and Spatial Variability of Ecosystem-  
581 Scale Carbon Dioxide, Water Vapor, and Energy Flux Densities. *Bull. American Met. Soc.* **82**, 2415-  
582 2434.
- 583 Balsamo, G., Bouyssel, F. and Noilhan, J., 2004. A simplified bi-dimensional variational analysis of soil  
584 moisture from screen-level observations in a mesoscale numerical weather-prediction model. *Q. J. R.*  
585 *Meteorol. Soc.*, **130**, 895-915.
- 586 Balsamo, G., Bouyssel, F., Noilhan, J., Mahfouf, J.-F., Bélair, S., Deblonde, G., 2005. A simplified  
587 variational analysis scheme for soil moisture: Developments at Météo-France and MSC,  
588 *ECMWF/ELDAS workshop on Land Surface Assimilation. ECMWF proceedings.* ECMWF, Reading,  
589 UK, 79-96.



590 Bastiaanssen, W.G.M., 1995. Regionalization of surface flux densities and moisture indicators in composite  
591 terrain : a remote sensing approach under clear skies in Mediterranean climates. Thesis, SC-DLO,  
592 Wageningen, 273 pp.

593 Bell, V.A., Blyth, E.M. and Moore, R.J., 2005. The use of soil moisture in hydrological forecasting,  
594 ECMWF/ELDAS workshop on Land Surface Assimilation. ECMWF - Proceedings. ECMWF,  
595 Reading, pp. 147-152.

596 Betts, A.K. and P. Viterbo, 2005. Land-surface, boundary layer and cloud-field coupling over the  
597 southwestern Amazon in ERA-40. *J. Geophys. Res.*, **110**, D14108, doi: 10.1029/2004JD005702.

598 Courtier, P., C. Freydl, J.F. Geleyn, F. Rabier and M. Rochas, 1991. The ARPEGE project at Météo-  
599 France. *Proc. ECMWF Seminar 2*, 193-232.

600 Denmead, O.T. and Shaw, R.H., 1962. Availability of Soil Water to Plants as Affected by Soil Moisture  
601 Content and Meteorological Conditions. *Agron. Journal*, **54**: 385.

602 Dirmeyer, P.A., F.J. Zeng, A. Ducharne, J.C. Morrill and R.D. Koster, 2000. The sensitivity of surface fluxes  
603 to soil water content in three land surface schemes. *J. Hydrometeorology* **1**, 121-134.

604 Doms, G., J. Foerstner, E. Heise, H.-J. Herzog, M. Raschendorfer, R. Schrodin, T. Reinhardt and G. Vogel,  
605 2005. *A description of the Nonhydrostatic Regional Model LM, Part II: Parameterization*. 140 pp.  
606 DWD, Offenbach. Also: <http://cosmo-model.cscs.ch/public/documentation.htm#p2>

607 Doms, G. and U. Schättler, 2002. *A Description of the Non-Hydrostatic Regional Model LM, Part I:*  
608 *Dynamics and Numerics*. 134 pp. Also: <http://cosmo-model.cscs.ch/public/documentation.htm#p1>.

609 Douville, H., Viterbo, P., Mahfouf, J.F. and Beljaars, A.C.M., 2000. Evaluation of the optimum interpolation  
610 and nudging techniques for soil moisture analysis using FIFE data. *Mon. Weather Rev.* **128**, 1733-1756.

611 Ek, M.B. and Holtslag, A.A.M., 2004. Influence of Soil Moisture on Boundary Layer Cloud Development. *J.*  
612 *Hydrometeorology* **5**, 86-99.

613 Hess, R., 2001. Assimilation of screen level observations by variational soil moisture analysis. *Meteorol.*  
614 *Atm. Phys.* **77**, 145-154.

615 Houser, P.R., Shuttleworth, W.J., Famiglietti, J.S., Gupta, H.V., Syed, K.H., Goodrich, D.C., 1998.  
616 Integration of soil moisture remote sensing and hydrologic modeling using data assimilation. *Water*  
617 *Resour. Res.* **34**, 3405-3420.

618 Jacobs, C.M.J. and De Bruin, H.A.R., 1992. The Sensitivity of Regional Transpiration to Land-Surface  
619 Characteristics - Significance of Feedback. *J. Clim.* **5**, 683-698.

620 Jarvis, P.G., 1976. The interpretation of leaf water potential and stomatal conductance found in canopies in  
621 the field. *Phil. Trans. R. Soc. Lond. B.* **273**, 593-610.

622 Jarvis, P.G. and McNaughton, K.G., 1986. Stomatal Control of Transpiration - Scaling up from Leaf to  
623 Region. *Adv. Ecol. Res.* **15**, 1-49.

624 Lindhardt, B., Abildtrup, C., Vosgerau, H., Olsen, P., Torp, S., Iversen, B.V., Jørgensen, J.O., Plauborg, F.,  
625 Rasmussen, P., Gravesen, P., 2001. *The Danish Pesticide Leaching Assessment Programme. Site*  
626 *Characterization and Monitoring Design*. Geological Survey of Denmark and Greenland, Copenhagen,  
627 74 pp.

628 Loveland, T.R., Reed, B.C., Brown, J.F., Ohlen, D.O., Zhu, Z., Young, L., Merchant, J.W., 2000.  
629 Development of a global land cover characteristics database and IGBP DISCover from 1 km AVHRR  
630 data. *Int. J. Remote Sensing* **21**, 1303-1330.

631 Mahfouf, J.F., 1991. Analysis of Soil-Moisture from near-Surface Parameters - a Feasibility Study. *J. Appl.*  
632 *Meteorol.* **30**, 1534-1547.

633 Masson, V., Champeaux, J.-L., Chauvin, F., Meriguet, C. and Lacaze, R., 2003. A Global Database of Land  
634 Surface Parameters at 1-km Resolution in Meteorological and Climate Models. *J. Clim.* **16**, 1261-1282.

635 Meetschen, D., van den Hurk, B., Ament, F. and Drusch, M., 2004. Optimized surface radiation fields  
636 derived from Meteosat imagery and a regional atmospheric model. *J. Hydromet.* **5**, 1091-1101.

637 Meijninger, W.M.L., Green, A.E., Hartogensis, O.K., Kohsiek, W., Hoedjes, J.C.B., Zuurbier, R.M., De  
638 Bruin, H.A.R., 2002. Determination of Area-Averaged Water Vapor Fluxes with Large Aperture and  
639 Radio Wave Scintillometers over a Heterogeneous Surface &ndash; Flevoland Field Experiment.  
640 *Boundary-Layer Meteorol.* **105**, 63-83.

641 Mitchell, K.E., Lohmann, D., Houser, P.R., Wood, E.F., Schaake, J.C., Robock, A., Cosgrove, B.A.,  
642 Sheffield, J., Duan, Q.Y., Luo, L.F., Higgins, R.W., Pinker, R.T., Tarpley, J.D., Lettenmaier, D.P.,  
643 Marshall, C.H., Entin, J.K., Pan, M., Shi, W., Koren, V., Meng, J., Ramsay, B.H., Bailey, A.A., 2004.  
644 The multi-institution North American Land Data Assimilation System (NLDAS): Utilizing multiple  
645 GCIP products and partners in a continental distributed hydrological modeling system. *J. Geophys. Res.*  
646 **109**, D07S90, doi:10.1029/2003JD003823.

647 Moene, A. and De Bruin, H.A.R., 2001. Sensible heat flux data derived from the scintillometers. *In: Z. Su*  
648 *and C. Jacobs (Editors), Advanced Earth Observations - Land Surface Climate, Final Report*. BCRS  
649 Reports. Ministry of Transport, The Hague, 85-90.

650 Noilhan, J. and Mahfouf, J.-F., 1996. The ISBA land surface parameterisation scheme. *Global and Planetary*  
651 *Change* **13**, 145-159.

652 Priestley, C.H.B. and Taylor, R.J., 1972. On the Assessment of Surface Heat Flux and Evaporation Using  
653 Large-Scale Parameters. *Mon. Weather Rev.* **100**, 81-92.

654 Raschke, E., Meywerk, J., Warrach, K., Andrea, U., Bergstrom, S., Beyrich, F., Bosveld, F., Bumke, K.,  
655 Fortelius, C., Graham, L.P., Gryning, S.-E., Halldin, S., Hasse, L., Heikinheimo, M., Isemer, H.-J.,  
656 Jacob, D., Jauja, I., Karlsson, K.-G., Keevallik, S., Koistinen, J., van Lammeren, A., Lass, U.,  
657 Launianen, J., Lehmann, A., Liljebladh, B., Lobmeyr, M., Matthaus, W., Mengelkamp, T., Michelson,  
658 D.B., Napiorkowski, J., Omstedt, A., Piechura, J., Rockel, B., Rubel, F., Ruprecht, E., Smedman, A.-S.,  
659 Stigebrandt, A., 2001. The Baltic Sea Experiment (BALTEX): A European Contribution to the  
660 Investigation of the Energy and Water Cycle over a Large Drainage Basin. *Bull. Amer. Met. Soc.* **82**,  
661 2389-2413.

662 Rhodin, A., Kucharski, F., Callies, U., Eppel, D.P. and Wergen, W., 1999. Variational analysis of effective  
663 soil moisture from screen-level atmospheric parameters: application to a short-range weather forecast  
664 model. *Q. J. R. Meteorol. Soc.* **125**, 2427-2448.

665 Rodell, M., Houser, P.R., Jambor, U., Gottschalck, J., Mitchell, K., Meng, C.J., Arsenault, K., Cosgrove, B.,  
666 Radakovich, J., Bosilovich, M., Entin, J.K., Walker, J.P., Lohmann, D., Toll, D., 2004. The global land  
667 data assimilation system. *Bull. Amer. Met. Soc.* **85**, 381-394.

668 Rubel, F., Brugger, K., Skomorowski, P. and Kottek, M., 2005. Daily and 3-hourly Quantitative Precipitation  
669 Estimation for ELDAS, *ECMWF/ELDAS workshop on Land Surface Assimilation. ECMWF -*  
670 *Proceedings*. ECMWF, Reading, 19-32.

671 Santanello, J.A., Friedl, M.A. and Kustas, W.P., 2005. An empirical investigation of convective planetary  
672 boundary layer evolution and its relationship with the land surface. *J. Appl. Meteorol.* **44**, 917-932.

673 Teuling, A.J., Uijlenhoet, R., Hupet, F. and Troch, P.A., 2006. Impact of plant water uptake strategy on soil  
674 moisture and evapotranspiration dynamics during drydown. *Geophys. Res. Lett.* **33**, L03401,  
675 doi:03410.01029/02005GL025019.

676 Uppala, S.M., Kallberg, P.W., Simmons, A.J., Andrae, U., Bechtold, V.D., Fiorino, M., Gibson, J.K.,  
677 Haseler, J., Hernandez, A., Kelly, G.A., Li, X., Onogi, K., Saarinen, S., Sokka, N., Allan, R.P.,  
678 Andersson, E., Arpe, K., Balmaseda, M.A., Beljaars, A.C.M., Van De Berg, L., Bidlot, J., Bormann,  
679 N., Caires, S., Chevallier, F., Dethof, A., Dragosavac, M., Fisher, M., Fuentes, M., Hagemann, S.,  
680 Holm, E., Hoskins, B.J., Isaksen, L., Janssen, P., Jenne, R., McNally, A.P., Mahfouf, J.F., Morcrette,  
681 J.J., Rayner, N.A., Saunders, R.W., Simon, P., Sterl, A., Trenberth, K.E., Untch, A., Vasiljevic, D.,  
682 Viterbo, P., Woollen, J., 2005. The ERA-40 re-analysis. *Q. J. R. Meteorol. Soc.* **131**, 2961-3012.

683 Valentini, R., Matteucci, G., Dolman, A.J., Schulze, E.D., Rebmann, C., Moors, E.J., Granier, A., Gross, P.,  
684 Jensen, N.O., Pilegaard, K., Lindroth, A., Grelle, A., Bernhofer, C., Grunwald, T., Aubinet, M.,  
685 Ceulemans, R., Kowalski, A.S., Vesala, T., Rannik, U., Berbigier, P., Loustau, D., Guomundsson, J.,  
686 Thorgeirsson, H., Ibrom, A., Morgenstern, K., Clement, R., Moncrieff, J., Montagnani, L., Minerbi, S.,  
687 Jarvis, P.G., 2000. Respiration as the main determinant of carbon balance in European forests, 2000.  
688 Respiration as the main determinant of carbon balance in European forests. *Nature* **404**, 861-865.

689 Van Den Hurk, B.J.J.M., 2002. European LDAS established. *Gewex Newsletter* **12**, 9.

690 Van Den Hurk, B.J.J.M., Bastiaanssen, W.G.M., Pelgrum, H. and Van Meijgaard, E., 1997. A new  
691 methodology for assimilation of initial soil moisture fields in weather prediction models using Meteosat  
692 and NOAA data. *J. Appl. Meteorol.* **36**, 1271-1283.

693 Van Den Hurk, B.J.J.M., Viterbo, P., Beljaars, A.C.M. and Betts, A.K., 2000. *Offline validation of the*  
694 *ERA40 surface scheme*. Technical Memorandum 295, ECMWF, Reading, 42pp.

695 Van Den Hurk, B.J.J.M., Viterbo, P. and Los, S.O., 2003. Impact of leaf area index seasonality on the annual  
696 land surface evaporation in a global circulation model. *J Geophys Res-Atmos* **108** (D6), 4191,  
697 doi:10.1029/2002JD002846.

698 Van den Hurk, B.J.J.M., and Ettema, J., 2007. Analysis of Soil Moisture Changes in Europe during a Single  
699 Growing Season in a New ECMWF Soil Moisture Assimilation System. *J. Hydromet.* (in press).

700 Viterbo, P., 1996. *The representation of surface processes in general circulation models*, ECMWF, Reading,  
701 201 pp.

702 Wergen, W., Hess, R. and Lange, M., 2005. Variational soil assimilation at DWD, *ECMWF/ELDAS*  
703 *workshop on Land Surface Assimilation. ECMWF - Proceedings*. ECMWF, Reading, 69-77.

704

**Table 1.** Summary of the setup of the ELDAS DA experiment.

NWP Centre	SVAT scheme	Land-surface database	Forcings ( $P, SW, LW$ )	Soil Moisture Assimilation
<i>CNRM</i>	ISBA	Ecoclimap	Model	$T, RH, (ELDAS P)$
<i>DWD</i>	TERRA	Ecoclimap	Model	$T$
<i>ECMWF</i>	TESSEL	GLCC	ELDAS	$T, RH$

**Table 2.** Water holding capacity (mm) for different soil types in ISBA, TERRA and TESSEL. Here, water holding capacity is defined as the difference between field capacity and wilting point for a 1-m deep layer of soil.

Soil	ISBA	TERRA	TESSEL
<i>Sand</i>	73	154	
<i>Sandy loam</i>	82	160	
<i>Loam</i>	88	230	152
<i>Loamy clay</i>	89	185	
<i>Clay</i>	85	206	

**Table 3.** Components of the soil hydrological balance of the upper meter in the soil at validation site El Saler, given as sums over the period DOY 162-191.  $P$  is the precipitation;  $E$  is the evapotranspiration;  $\delta W$  represents the increments due to the data assimilation;  $\Delta S_{1m}$  is the storage change of water in the upper 1 m of the soil; “Other” includes runoff, drainage and changes in water storage of layers below 1 m.

	DATA	ISBA	TERRA	TESSEL
<b>P (mm)</b>	2	3	3	0
<b>E (mm)</b>	-41	-116	-107	-69
<b><math>\delta W</math> (mm)</b>		122	80	27
<b><math>\Delta S_{1m}</math> (mm)</b>		7	-17	-32
<b>Other</b>		-2	7	10

**Table 4.** Mean monthly bias (model-observations) and rmse in P-E and P-E+ $\delta W$ , respectively, for ISBA, TERRA and TESSEL, computed for the period May-October 2000.

	Bias P-E (mm)	Bias P-E+ $\delta W$ (mm)	rmse P-E (mm)	rmse P-E+ $\delta W$ (mm)
<i>ISBA</i>	-24.7	-6.0	53.4	44.6
<i>TERRA</i>	-33.6	-5.8	55.5	52.7
<i>TESSEL</i>	-13.1	-0.9	28.1	24.0

**Table 5.** Seasonal mean of bias and rmse in  $\Lambda$  from errors on a monthly timescale as well as the seasonal rmse in  $\Lambda$  from errors on a daily timescale. Months included are May-September.

	Bias $\Lambda$ (monthly)	<i>rmse</i> $\Lambda$ (monthly)	<i>Rmse</i> $\Lambda$ (daily)
<i>ISBA</i>	0.085	0.23	0.27
<i>TERRA</i>	0.060	0.21	0.24
<i>TESSEL</i>	0.066	0.20	0.24

### ELDAS validation sites

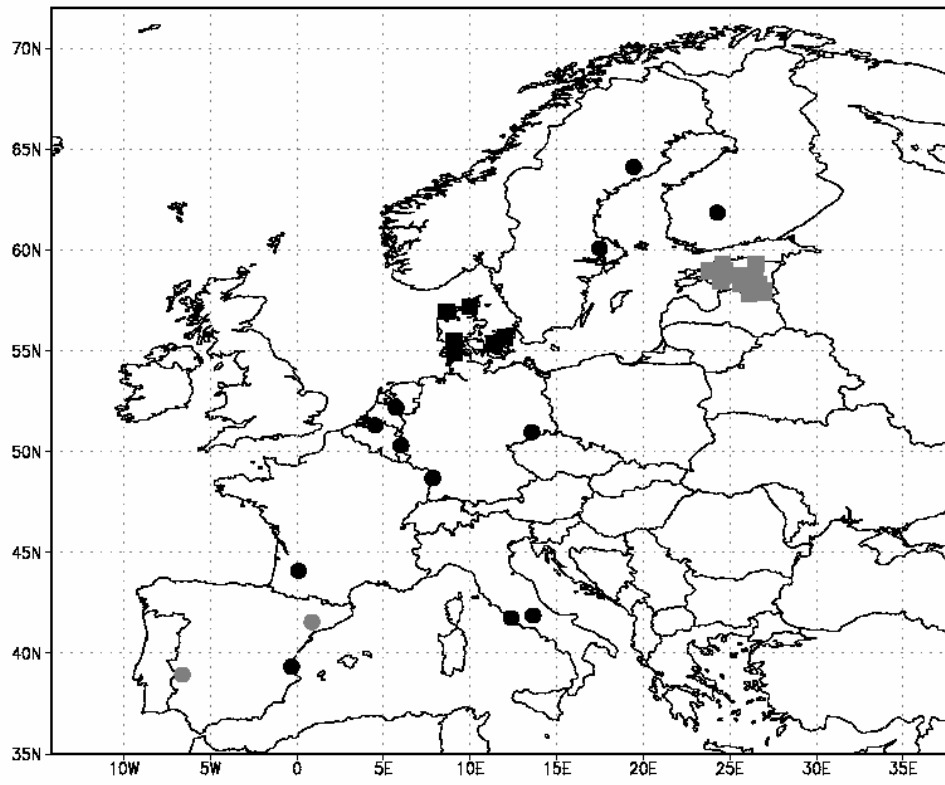


*Figure 1. Location of the ELDAS validation sites Black circles CarboEurope sites; Grey circles: Scintillometer sites; Black squares: PLAP sites; Grey squares: BALTEX sites. See text for a further description of the sites.*

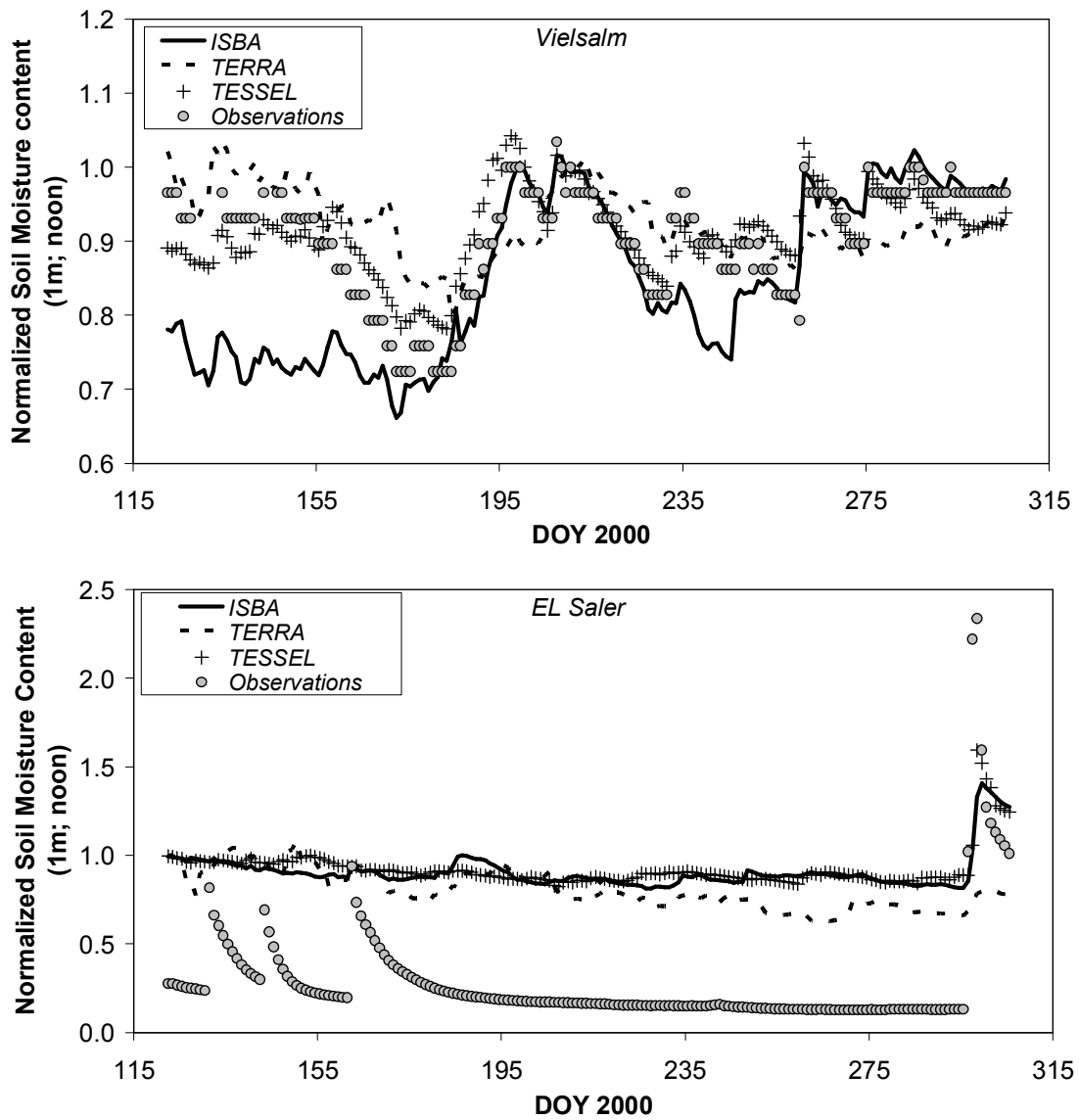


Figure 2. Normalized modelled and observed soil moisture content  $\hat{\theta}$  for the validation sites El Saler (upper) and Vielsalm (lower), respectively, during the validation period. Note the difference in scale.



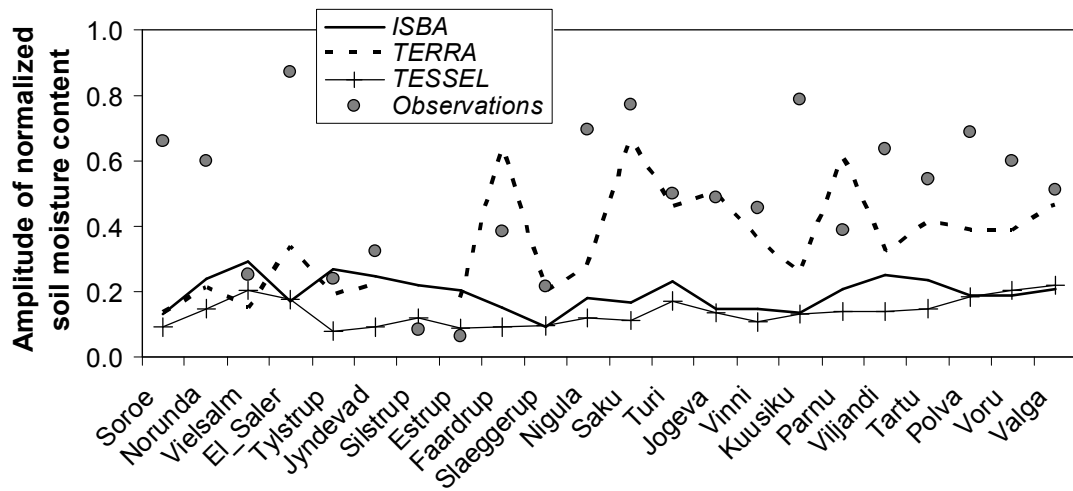


Figure 3. Comparison of observed and modelled amplitudes of the normalized soil moisture content  $\hat{\theta}$ . Labels on the x-axis denote the validation sites. The model outputs are connected by a line to facilitate comparison with the data.

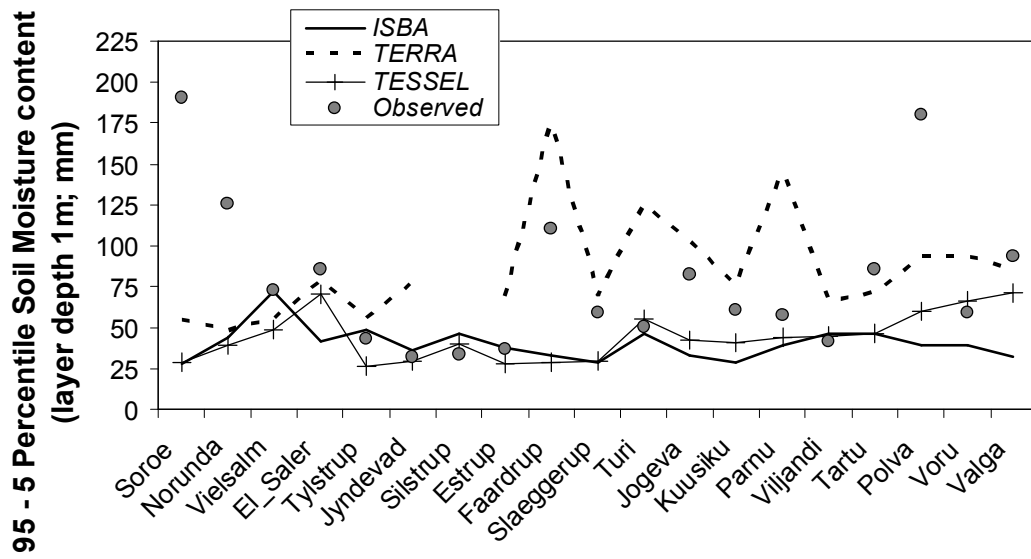


Figure 4. Comparison of observed and modelled amplitudes of the soil moisture content in the upper meter of the soil. In contrast with the amplitude shown in Fig. 3, the amplitude is defined here as the difference between the 95 and 5 percentile daily values, respectively, in the validation period (May-October 2000). Labels on the x-axis denote the validation sites. The model outputs are connected by a line to facilitate comparison with the data.

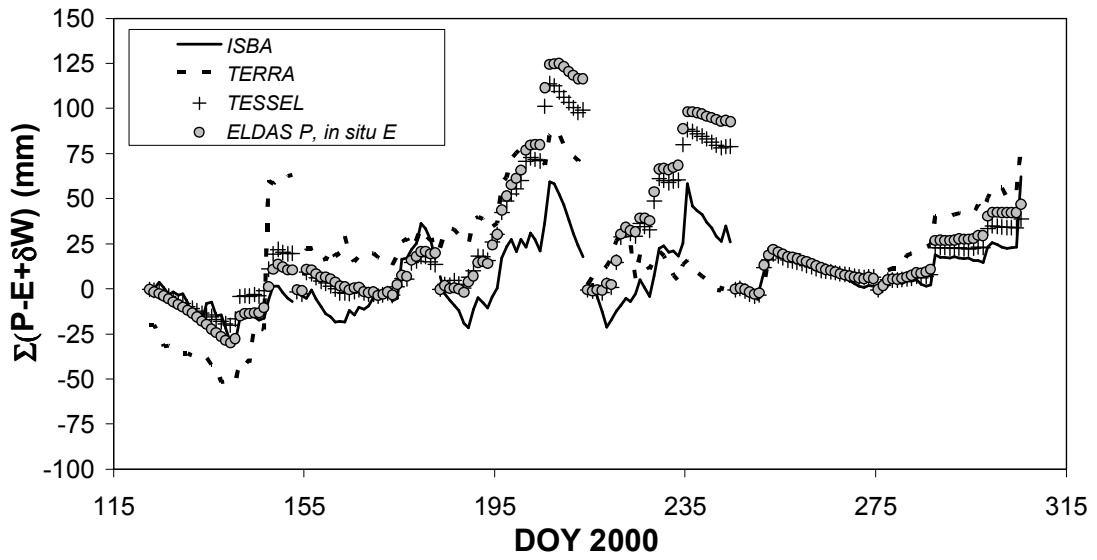
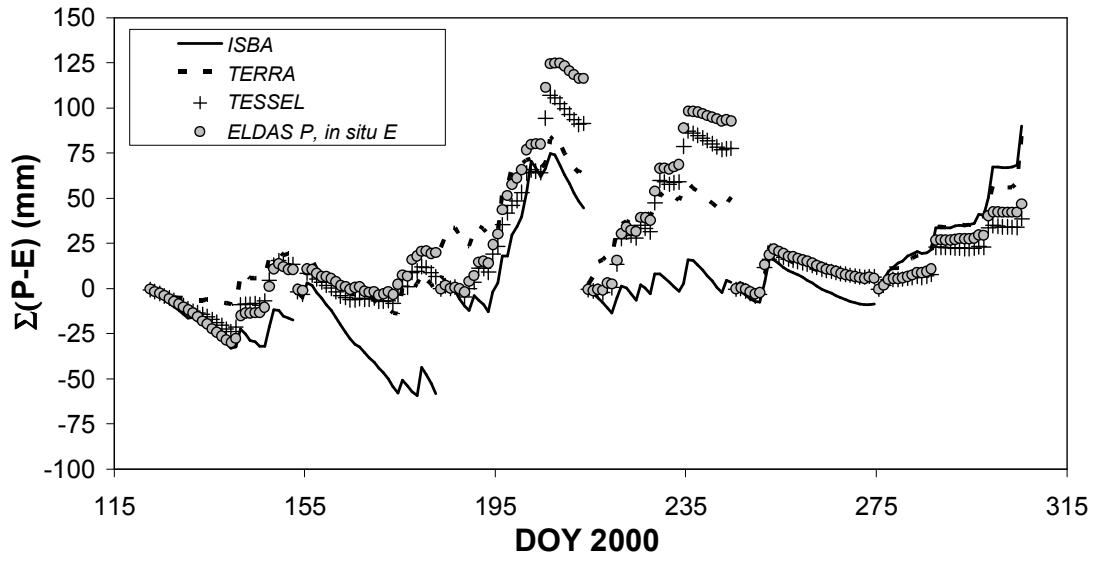


Figure 5. Illustration of the effect of the data assimilation increments on the soil hydrological balance. Case study Flakaliden (Sweden). Upper:  $P-E$ ; Lower:  $P-E$  for the data and  $P-E+\delta W$  for the models.  $\delta W$  denotes the contribution from the data assimilation. Values shown are cumulative values, reset to zero at the start of each month.

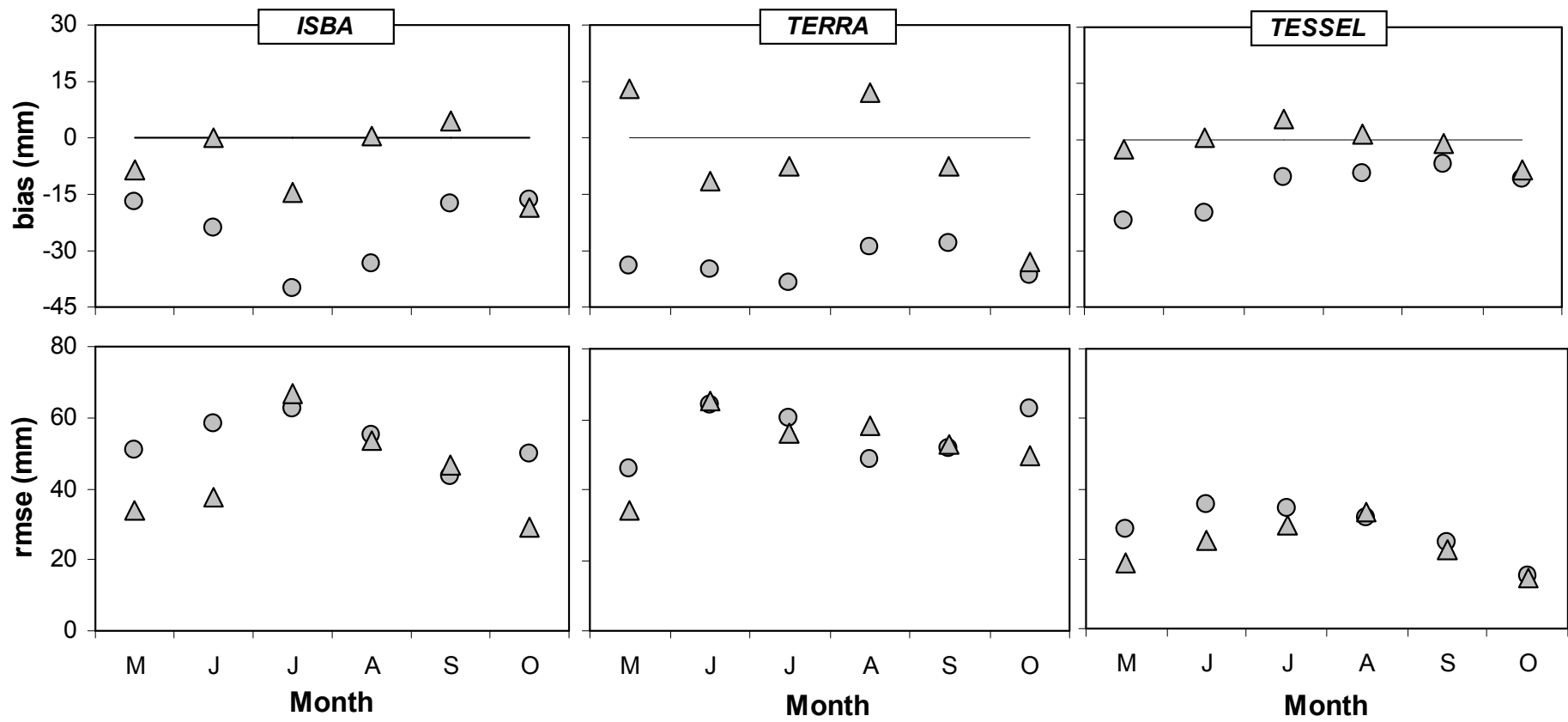


Figure 6. Bias (model-observations) and rmse of monthly sums of P-E (circles) and P-E+ $\delta W$  (triangles) for ISBA (left), TERRA (middle) and TESSEL (right), respectively.

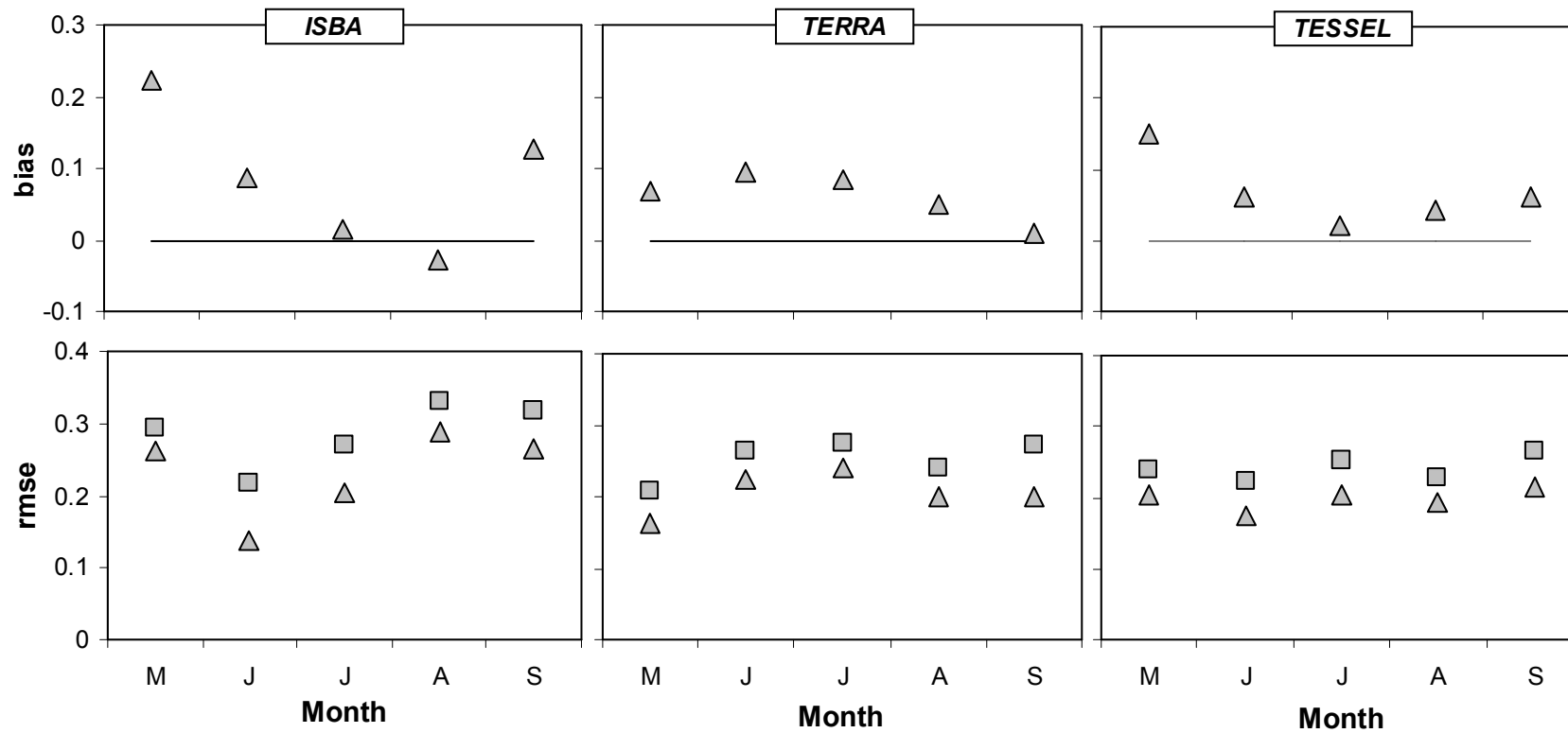


Figure 7. Bias (model-observations) and rmse of the evaporative fraction  $\Lambda$  on a monthly timescale (triangles) for ISBA (left), TERRA (middle) and TESSEL (right), respectively. Also shown in the lower panels is the rmse of  $\Lambda$  on a daily timescale (squares).

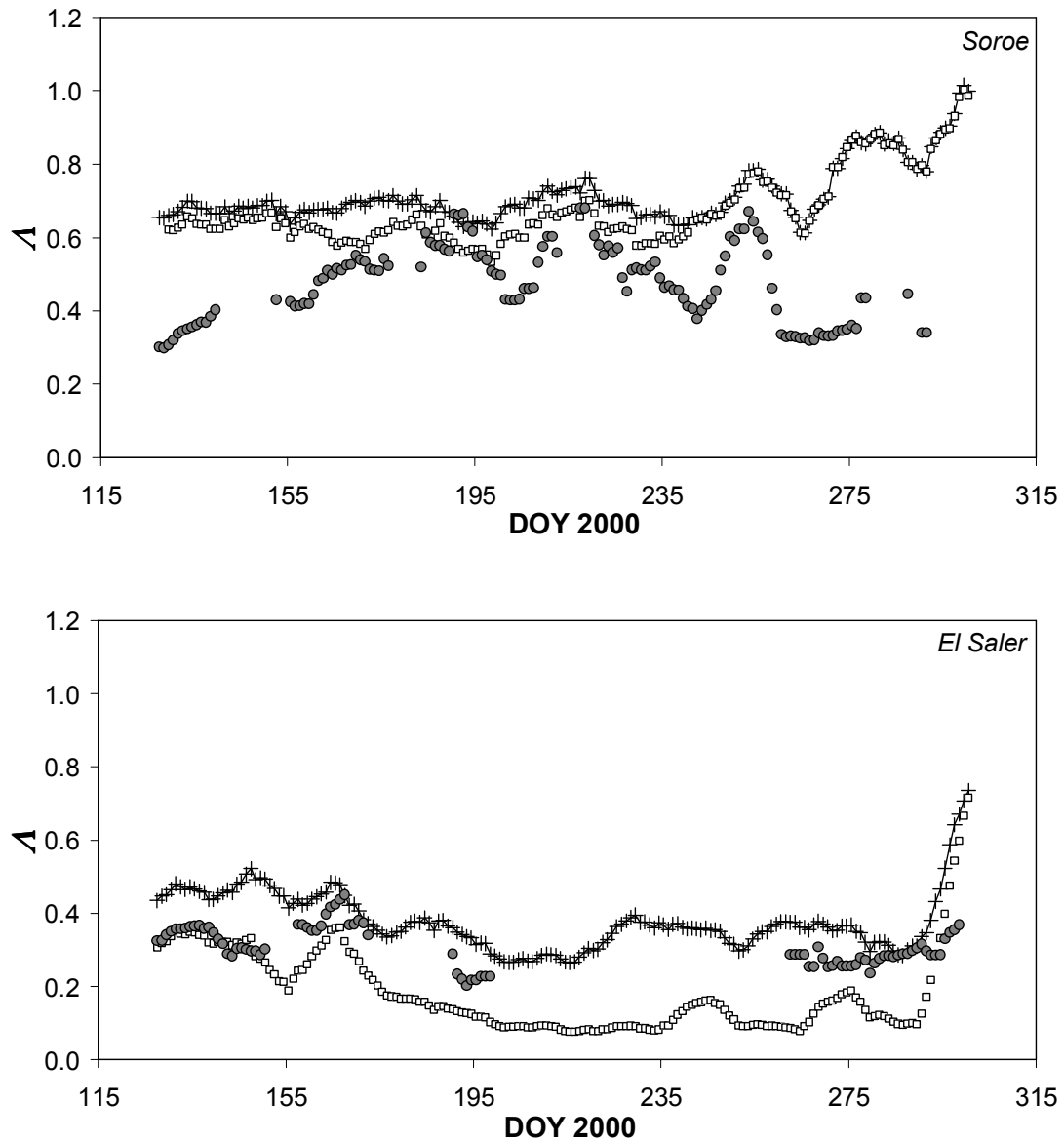


Figure 8. Illustration of the impact of the TESSEL DA system on the evaporative fraction  $\Lambda$  for a typical moist and dry case, respectively. Upper panel: moist case (Soroe, Denmark); Lower panel: Dry case (El Saler, Spain). Filled circles: observations; pluses: TESSEL with DA system; squares: TESSEL

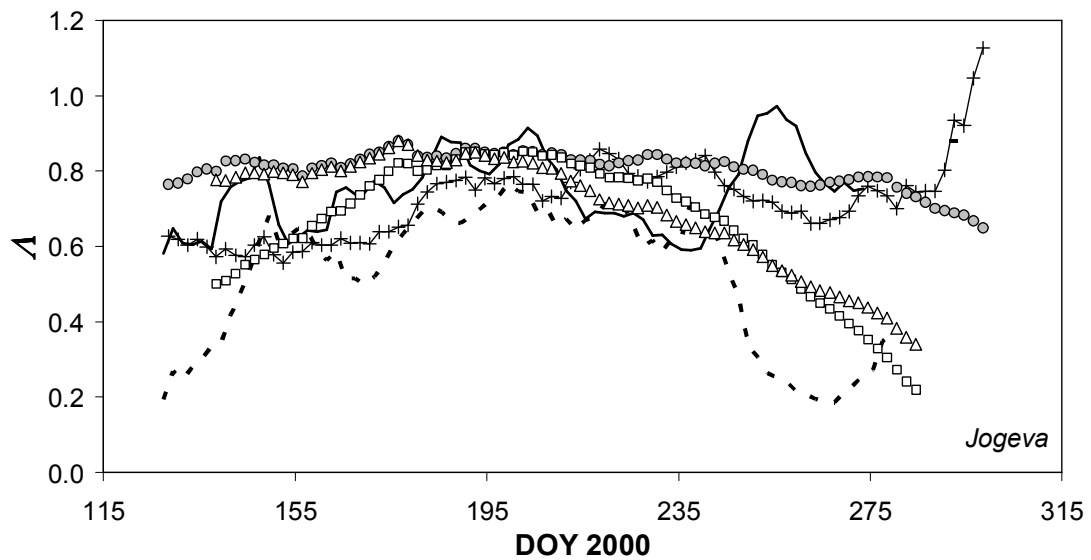


Figure 9. Illustration of the possible impact of surface properties on model output for  $\Lambda$ , case Jogeva, Estonia. The curves show 11-day moving averages of the evaporative fraction  $\Lambda$  around noon (see text). Black line: ISBA; dashed line: TERRA; pluses: TESSEL; open circles:  $\Lambda_{PT}$ ; triangles:  $\Lambda_{PT}$  multiplied by  $LAI/LAI_m$  from ISBA; horizontal dashes:  $\Lambda_{PT}$  multiplied by  $LAI/LAI_m$  from TERRA.